Registering Retinal Vessel Images from Local to Global via Multiscale and Multicycle Features

Haiyong Zheng[1] Lin Chang[1] Tengda Wei[1] Xinxin Qiu[1] Ping Lin[2] Yangfan Wang[1]
[1]Ocean University of China [2]The University of Dundee
zhenghaiyong@ouc.edu.cn
{changlinok1234, tdwei123, qxx1990421}@163.com, plin@maths.dundee.ac.uk, yfwang@ouc.edu.cn

Abstract

We propose a comprehensive method using multiscale and multicycle features for retinal vessel image registration with a local and global strategy. The multiscale vessel maps generated by multiwavelet kernels and multiscale hierarchical decomposition contain segmentation results at varying image resolutions in different levels of vessel details. Then the multicycle feature composed of various combinations of cycle structures with different numbers of vertices is extracted. The cycle structure consisting of vessel bifurcation points, crossover points of arteries and veins, and the connected vessels can be found by our Angle-based Depth-First Search (ADFS) algorithm. Local initial registration is implemented by the matched Cycle-Vessel feature points and global final registration is completed by the Cycle-Vessel-Bifurcation feature points using similarity transformation. Finally, our Skeleton Alignment Error Measure (SAEM) is calculated for optimal scale and cycle feature selection, yielding the best registration result intelligently. Experimental results show that our method outperforms state-of-the-art methods on retinal vessel image registration using different features in terms of accuracy and robustness.

1. Introduction

Retinal vessel images contain valuable local and time information as they are usually acquired from different modalities over many years, which can be aligned to one image by image registration to aid ophthalmologists for analysis and diagnosis of various diseases such as diabetic retinopathy, age-related macular degeneration, and glaucoma. In this paper, we focus on accurate and robust feature-based retinal image registration.

The registration methods can be classified into intensity-based and feature-based [13]. Intensity-based methods generally optimize a similarity measure based on cross-correlation, phase correlation, and mutual information, etc. [17], which will take great computation cost to find the optimal solution, especially they need to incorporate the whole image information to finish the registration. Also, the intensity-based methods may fail to align the images if the image quality is quite low or the overlapping region between the images is small. These motivate the exploitation of robust features such as retinal vessel and optic disk instead of intensity in retinal image registration [16]. Most of the feature-based methods use bifurcation for registration since it is a prominent indicator of vasculature. Zana and Klein [23] used bifurcation points with surrounding vessel orientations for multimodal registration. Can and Stewart [2] proposed a hierarchical algorithm using branching points and crossover points in the retinal vasculature to avoid unmatchable image features and mismatches between features, and then it was extended to Dual-Bootstrap Iterative Closest Point (ICP) algorithm that iteratively decides the optimal transformation model from simple to complex and expands the bootstrap region from local to global [20]. The blood vessel bifurcations were also identified as control points to evaluate the transformation types and the pixel-level fusion techniques [11]. Chanwimaluang *et al.* [4] proposed a hybrid retinal image registration approach that combines both area-based and feature-based methods using crossover/bifurcation points of vascular tree as landmark points. And the RERBEE algorithm was presented with BEES representing the vasculature structure (bifurcations and segments) for registration [18]. These methods largely depend on the branching angles of single bifurcation/crossover point, and these features have coarse precision leading to matching which may not be unique and reliable for registration purpose.

Compared with the aforementioned point-matching methods, structure-matching registration is favored to overcome the possible mismatches. Chen *et al.* [6, 5] presented a bifurcation structure composed of a master bifurcation point and its three connected neighboring pixels or vessel segments, with the normalized branching angle and length as its characteristic vector. Shen *et al.* [19] then extended

bifurcation structure-matching by a local fine registration. However, bifurcation structure is still not unique and reliable enough for registration that may make the matching missed if the vascular tree is detailed, especially followed by the vessel segmentation result in one scale.

In view of this, we propose the cycle structure for feature-based retinal image registration. The cycle structure, consisting of vessel bifurcation points, crossover points of arteries and veins, and the connected vessels, is more unique, reliable and invariant against translation, rotation, and scaling, especially for the retina from the same person over many years, so it can also be used in many other applications such as retina identification [1] and verification [10]. To overcome the dependence on the vessel segmentation for registration, we use multiwavelet kernels and multiscale hierarchical decomposition [22] to generate multiscale vessel maps at varying image resolutions in different levels of vessel details and then adopt our Angle-based Depth-First Search (ADFS) algorithm to extract the multicycle feature composed of various combinations of cycle structures with different numbers of vertices. For regions away from the matching cycles, we implement the two-stage registration from local to global to construct the robust Cycle-Vessel-Bifurcation feature for final registration using similarity transformation. Finally, our Skeleton Alignment Error Measure (SAEM) is calculated for optimal scale and cycle feature selection, yielding the best registration result. Figure 1 shows the framework of our proposed method.

The rest of the paper is organized as follows: Section 2 gives our multiscale segmentation and skeleton method for retinal vessel images; the detection, extraction, description and matching of our proposed cycle structure are presented in Section 3; and Section 4 introduces our two-stage local-to-global strategy for accurate registration; then our SAEM is proposed in Section 5 to obtain the best registration result automatically; Section 6 shows the qualitative and quantitative experimental results and Section 7 concludes this paper.

2. Multiscale Segmentation and Skeleton

Due to hardware limitations, retinal images usually have characteristics of uneven illumination, large numbers of noise points, and low contrast between vessels and background, which lead to the challenge of automatic analysis. Retinal vessel segmentation plays a key role on the accuracy of registration.

In this work, multiwavelet kernels and multiscale hierarchical decomposition method [22] is used for multiscale vessel segmentation. And 14 vessel maps are generated at varying image resolutions representing different levels of vessel details to avoid the possible failed feature extraction caused by single segmentation. We then remove the invalid scales using a threshold of pixel number for the segmentation results with very few vessel pixels because they obviously miss the important vessel information.

The multiscale segmentation results are further processed by the following procedures for better feature extraction: 1) remove the connected regions with few pixels recognized as non-vessel by a threshold for denoising; 2) fill the vessel holes caused by the central light reflex of retinal arteries and veins based on erosion and dilation method; 3) skeletonize the vessels to obtain one pixel width vascular tree using the contour-pruned skeletonization method [1].

The reference image and the floating image for registration are both segmented and skeletonized by the above multiscale processing, yielding up to 14 vessel skeleton results respectively (each $N_j, j = 1, 2, \cdots, 14$ needs to be aligned with each $M_i, i = 1, 2, \cdots, 14$ as shown in Figure 1). Figure 2 shows an example of the multiscale vessel segmentation and skeleton results.

3. Multicycle Matched Structure

The retinal vasculature, consisting of arteries and veins, and their end branches, forms capillary networks (see Figure 2), thus can be formally described as an unweighted graph G [9]. We then design and construct the cycle structure using vessel bifurcation points, crossover points of arteries and veins, and the connected vessels. Multicycle means that various combinations of cycle structures are segmented by multiscale hierarchical decomposition with different scales. In our work, the minimum cycles, defined as a cycle basis where the sum of the weights of the cycles is minimum [12], are selected for retinal image registration. The minimum cycle bases of a graph encapsulate the entire cycle space in a concise manner so that they are very useful in many contexts, e.g., structural engineering [3], cycle analysis of electrical networks [7], and chemical ring perception [8].

3.1. Cycle Structure Detection and Extraction

The extraction procedure of cycle structures can be implemented by two steps: searching feature points and finding cycle structures.

3.1.1 Searching Feature Points

The feature points we used for cycle structure consist of the bifurcation and crossover points in the binary skeleton vascular network, and they can be searched as follows:

1. Label the pixels whose sum of 8-adjacent pixels is greater than 2 into connected components, because the pixels cannot be bifurcation or crossover points if the sum of its 8-adjacent pixels is less than or equal to 2.

[1] http://www.cs.smith.edu/∼nhowe/research/code/

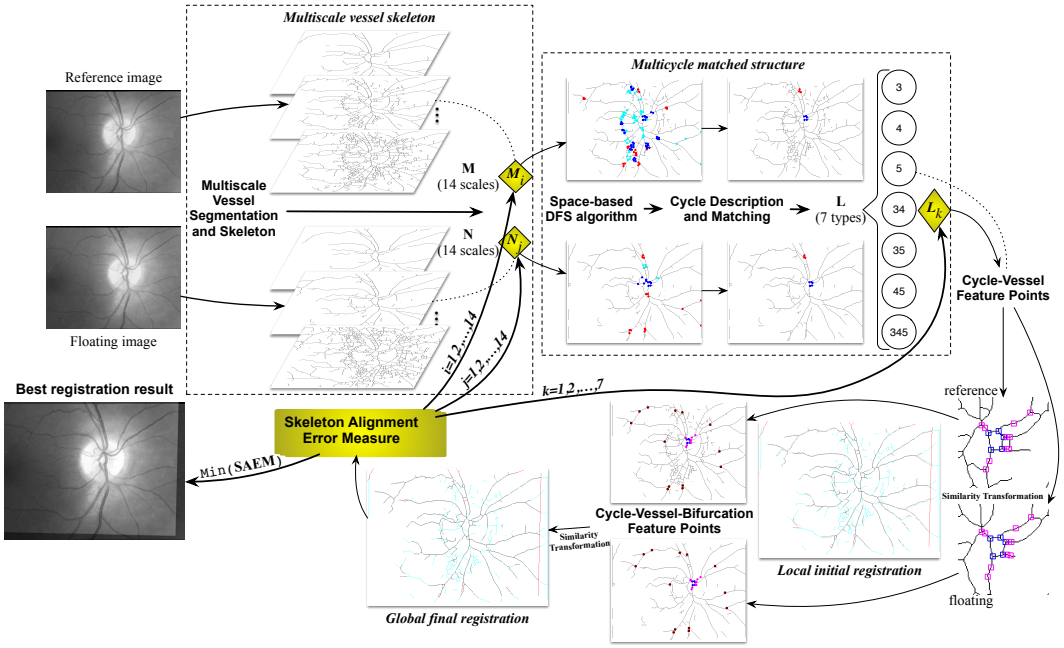

Figure 1. The framework of retinal vessel image registration from local to global via multiscale and multicycle features.

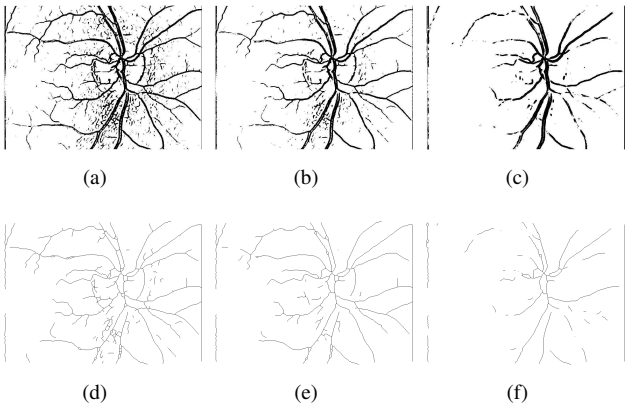

Figure 2. Multiscale vessel segmentation and skeleton results of a low contrast retinal image. (a), (b) and (c) are three segmentation results in three different scales, (d), (e) and (f) are the corresponding skeleton results, respectively.

2. Find the centroids of all the connected components and label them as candidate feature points, and they can be considered as vertices (nodes) while their connected vessels can be considered as edges (links) in graph theory.

3. Determine the feature points by removing the candidate vertices whose degree is equal to 1 iteratively, as a vertex belongs to a cycle only if it has at least two connected vertices.

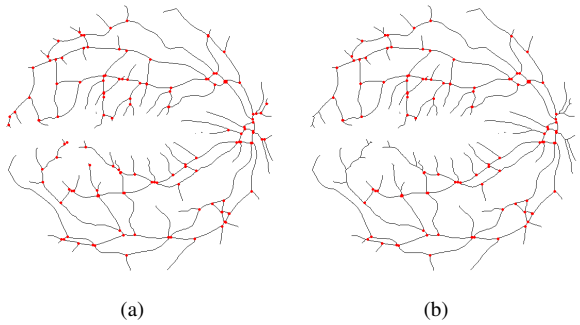

Figure 3. Searching feature points. (a) The candidate feature points, and (b) the feature points.

Figure 3 gives an example showing the candidate feature points and the feature points respectively.

3.1.2 Finding Cycle Structures

As mentioned above, finding the cycle structures from the vascular network is equivalent to computing the minimum cycle basis from the undirected and unweighted graph, but with the difference of that the feature points have fixed spatial position in the image while the vertices in the graph usually don't. Therefore, we take spatial information of feature points into consideration to develop the Angle-based Depth-First Search (**ADFS**) algorithm (Algorithm 1) for finding the cycle structures. Our ADFS algorithm can find

the minimum cycle basis of the image-based undirected and unweighted graph with 1 edge and n vertices effectively and efficiently by reducing the time complexity from $O(n/\log n+n^2)$ [12] to $O(n^2)$ due to the use of spatial (angle) information. According to the characteristics of retinal vasculature, only cycle structures composed of three, four and five feature points are chosen for registration in our work.

Algorithm 1 Angle-based Depth-First Search (ADFS)

Input: The feature points and their connectivities in the binary skeleton image.
Output: The cycle structures.

for all A such that $A \in FeaturePointsSet(P_n)$ **do**
  for all B such that $B \in P_n$ **and** connects to A **do**
    calculate the vector V_{BA}
    for all C such that $C \in P_n$ **and** connects to B **do**
      calculate the vector V_{BC}
      calculate the angle $\Theta_{ABC} = \angle ABC$
    end for
    determine C such that $\min(\Theta_{ABC})$
    if C connects to A **then**
      output $CycleStucture(ABC)$
      continue
    else
      repeat for all [$D \in P_n$ **and** connects to C]
      output $CycleStucture(ABCD)$ and continue
      or iterate next connected feature point
      until no connected feature point
    end if
  end for
end for

3.2. Cycle Structure Description and Matching

All the cycle structures found in the reference image and the floating image need to be matched to determine the **Cycle** feature points (on matched cycle structures) for transformation and further registration. In order to make the structure more unique and reliable for registration, we describe a cycle structure using branch lengths, branch angles, and angles between adjacent edges, among which branch angles represent the connected relationship of vessels on each feature point while angles between adjacent edges represent the relative position of feature points. Figure 4 shows an example description of a four-point cycle structure. The lengths are calculated based on the pixel distance and the angles are calculated relying on the adjacent points in the vessels or edges. Then we normalize all the lengths and angles by Equation 1 and 2 to preserve scaling invariant and guarantee rotation invariant respectively, yielding the final feature vector given in Equation 3 as an example corresponding to Figure 4.

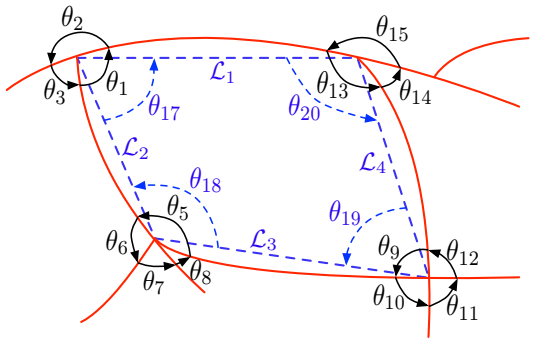

Figure 4. Cycle structure description. $\mathcal{L}_1 \sim \mathcal{L}_4$, $\theta_1 \sim \theta_{16}$ and $\theta_{17} \sim \theta_{20}$ represent branch lengths, branch angles and angles between adjacent edges respectively in a four-point cycle structure.

$$\mathcal{L}_{iNorm} = \frac{\mathcal{L}_i}{\sum \mathcal{L}} \tag{1}$$

$$\theta_{jNorm} = \frac{\theta_j}{360^\circ} \tag{2}$$

$$\tilde{v} = \{lengths, angles\} = \{\mathcal{L}_1, \mathcal{L}_2, \mathcal{L}_3, \mathcal{L}_4, \theta_1, \theta_2, \theta_3, \mathbf{0}, \theta_5, \theta_6, \theta_7, \theta_8, \theta_9, \theta_{10}, \theta_{11}, \theta_{12}, \theta_{13}, \theta_{14}, \theta_{15}, \mathbf{0}, \theta_{17}, \theta_{18}, \theta_{19}, \theta_{20}\} \tag{3}$$

The number of feature vector elements varies with the number of cycle feature points, and the number of branch angles varies with the style of feature points, e.g., a bifurcation point usually has 3 branch angles while a crossover point has 4 branch angles. To obtain consistent vector length for further matching, we consider the feature points of the cycle structure all as bifurcation or crossover points, making maximum 4 branch angles for each point and then the feature vector of three-, four- and five-point cycle structure becomes 18, 24, and 30 dimensions (the missing elements are set to 0 as demonstrated in Equation 3), respectively.

Matching two cycle structures with the same number of feature points can be implemented by minimizing the similarity measure $D_{pq} = mean(|V_p - W_q|)$, where V_p represents the p-th cycle structure in the reference image, W_q represents the q-th cycle structure in the floating image and the function $mean(\cdot)$ calculates the average value of vector. To avoid the possible mismatches even with the minimum D, a threshold is used to verify the matching again, so that one or more of the three-, four- and five-point cycle structures may be ignored, e.g., the four-point cycle structure is missed after the matching illustrated in Figure 1. This method tries to find the most accurate matching cycle structures between the reference and the floating while misses the others, so that the matched cycle feature points for registration are very accurate but not much in number. There-

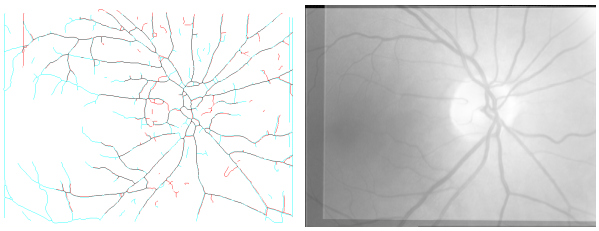

(a) (b)

Figure 5. Local initial registration. (a) is the skeleton image registration result, and (b) is the corresponding retinal image registration result.

fore, we combine all kinds of the matched cycle structures up to 7 types $L_k, k = 1, 2, \cdots, 7$ as shown in Figure 1, yielding the multicycle matched structure.

4. Registration from Local to Global

In order to get a more accurate registration, we design a two-stage local-to-global strategy using the **Cycle-Vessel** and **Cycle-Vessel-Bifurcation** feature points respectively.

4.1. Local Initial Registration

The multicycle matched structure only contains limited accurate cycle feature points, which may not be enough for further transformation and then registration. So we also extract the closest bifurcation points or ending points connected to the cycle feature points along the vessels and the midpoints of the vessels to constitute the **Cycle-Vessel** feature points for local initial registration.

It's obvious that the cycle-vessel structure is invariant against translation, rotation, and scaling, but is variant to shearing because of the angles between vessels, therefore, similarity transformation is the best choice. The similarity transformation can be defined by

$$X = xs\cos\varphi - ys\sin\varphi + \hat{a} \tag{4}$$

$$Y = xs\sin\varphi + ys\cos\varphi + \hat{b} \tag{5}$$

where s denotes scaling, φ denotes rotational, and $(\hat{a}, \hat{b})$ denotes translational differences between the reference image and the floating image. In our work, the least squares solution is adopted to obtain the transformation parameters [21]. Figure 5 shows the results of local initial registration using the cycle-vessel feature points.

4.2. Global Final Registration

Although the cycle-vessel feature points are very accurate for registration (Figure 5), it's still not robust enough because these points only cover vascular regions with intricate capillary that may make some global regions far away from them unaligned (Figure 6a and 6b). Therefore, we extend the registration from local to global by finding the unaligned bifurcation points from the local registration result to further constitute the final **Cycle-Vessel-Bifurcation** feature points.

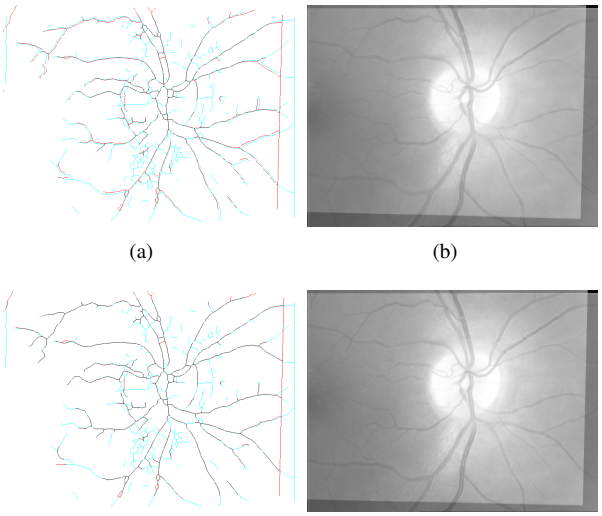

(a) (b)

(c) (d)

Figure 6. Comparison of local initial registration and global final registration. (a) and (b) are skeleton and retinal image results respectively by local initial registration with unaligned vessels in some local regions, while (c) and (d) are the comparative skeleton and retinal image results respectively after global final registration with better vessel alignment precisely.

The unaligned bifurcation points are determined by bifurcation matching and distance thresholding: 1) find the matching bifurcation point of each bifurcation point in the floating local registration image among its 5×5 neighborhood relying on the angles [23]; 2) regard the matched bifurcation points as unaligned if their pixel distance is greater than 3 pixels. Then, similar to local registration, the similarity transformation is adopted for final registration using the cycle-vessel-bifurcation feature points. Figure 6c and 6d show the global final registration results corresponding to the local registration results Figure 6a and 6b, which can be seen more precisely.

5. Skeleton Alignment Error Measure

One reference image and one floating image, also known as one pair of images for registration, will produce up to 14×14 multiscale vessel segmentation and skeleton results with up to 7 multicycle matched structures, yielding at most $14 \times 14 \times 7$ local-to-global registration results (Figure 1). We then define the Skeleton Alignment Error Measure (**SAEM**) and choose the optimal registration result automatically by minimizing SAEM as follows:

1. Given a reference skeleton result M_i (i =

$1, 2, \cdots, 14$) and a floating skeleton result N_j ($j = 1, 2, \cdots, 14$), N_j is aligned to M_i with one type of multicycle matched structure L_k ($k = 1, 2, \cdots, 7$) under the local-to-global strategy, yielding the transformed skeleton result N_{jM_i};

2. For each vessel point in N_{jM_i}, calculate the pixel distance d of its nearest vessel pixel among its 7×7 neighborhood in M_i, or mark this vessel point invalid if no corresponding vessel pixel is found;

3. SAEM is defined by $SAEM_{ijk} = (\sum d)/Num_v$, where Num_v is the number of valid pixels in N_{jM_i} that d can be calculated;

4. Constraints: $SAEM$ is considered valid only if $Num_v/Num_{N_j} \geq 50\%$ and $Num_{N_{jM_i}}/Num_{N_j} \geq 38\%$, where $Num_{(\cdot)}$ denotes the number of pixels in $(\cdot)$.

The constraints are necessary to exclude the extremely mismatching situations that may make the $SAEM$ minimized because of very few contributing pixels.

By using SAEM, the best registration result will be selected intelligently, moreover, the registration method can be evaluated. The overall framework of our proposed method for retinal vessel image registration can be seen in Figure 1.

6. Experiments

There exist rare public datasets of retinal images for registration purpose, so we use VARIA database [15, 14][2] that contains a set of retinal images for authentication purpose to evaluate and compare the performance of our method for retinal image registration qualitatively and quantitatively. The database currently includes 233 images from 139 different individuals that have been acquired with a TopCon non-mydriatic camera NW-100 model and are optic disc centered with a resolution of 768×584, among which 155 pairs from 59 individuals (total 153 images from all 233 retinal images) can be constructed as a new dataset for registration purpose[3].

6.1. Qualitative Results

Figure 7 shows two examples of our retinal vessel image registration from local to global via multiscale and multicycle features, among which (a)(b) and (f)(g) are two pairs of original retinal images for registration, (c) and (h) are the corresponding best registration results selected by our SAEM automatically, (d) and (i) are local initial registration results while (e) and (j) are global final registration results, respectively. Although the pairs of original retinal images are dramatically different with big deformation, it can still be seen that the final results Figure 7(c) and (h) are both well registered accurately by minimizing the SAEM via multiscale and multicycle features and robustly through the local-to-global strategy. The zoom-in regions on Figure 7(e) and (j) are shown obviously more precise of aligned vessels than those corresponding regions on Figure 7(d) and (i) respectively, indicating that the effectiveness and robustness of our two-stage local-to-global registration strategy.

6.2. Quantitative Results

For quantitative comparison, the Success Rate (**SR**) and Skeleton Alignment Error Measure (**SAEM**) are used to evaluate our method and other methods on the 155 pairs of retinal images. The registration is regarded as successful evaluated by the ophthalmologists considering the real medical applications for SR calculation ($SR = (\text{Successful Pairs})/155$) and the failed registration will be excluded to calculate $SAEM$.

First, the transformation models are important for different features of registration and have been discussed by [20, 11], and Table 1 shows the registration results with respect to our cycle structure using different transformation models[4]: similarity, affine, and second-order polynomial. Although the SAEM of polynomial transformation is minimum with 0.231 pixel, it's still not suitable for cycle structure due to the lowest SR (16.99%) because the failed registrations will not contribute to SAEM, which may make the SAEM very small based on very few successful registrations. Therefore, because the proposed cycle-vessel structure is invariant against translation, rotation, and scaling, but is variant to shearing due to the angles between vessels, the similarity transformation for our cycle structure is the best choice with the highest 96.73% SR and the acceptable 0.938 pixel SAEM for ophthalmologists.

Transformation models	SR	SAEM (pixel)
Similarity	**96.73%**	**0.938**
Affine	50.33%	1.010
Polynomial	16.99%	0.231

Table 1. Comparison of different transformation models.

Then, Table 2 shows the registration results by similarity transformation using different features on the 155 pairs of retinal images under the optimal $M_i N_j L_k$ with minimum $SAEM_{ijk}$: Cycle, Cycle-Vessel, and Cycle-Vessel-

[2] http://www.varpa.es/varia.html

[3] Only the two retinal images that belong to the same individual can be considered as one pair for registration.

[4] Only Cycle features are used in this experiment, and the 155 pairs of retinal images under the optimal $M_i N_j L_k$ with minimum $SAEM_{ijk}$ are selected for this experiment.

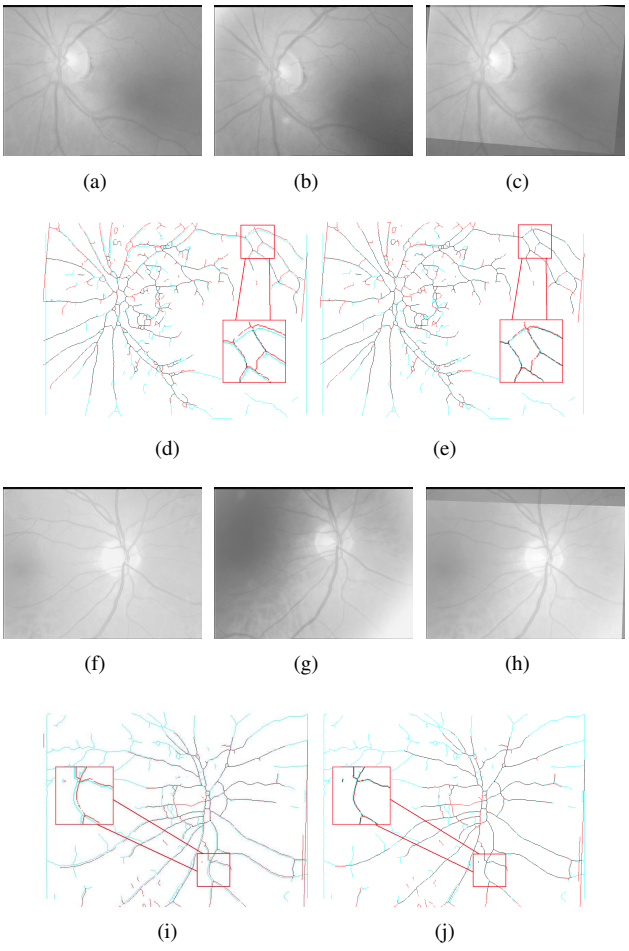

Figure 7. The qualitative results of our proposed retinal image registration. (a)(b) and (f)(g) are two pairs of original retinal images for registration, (c) and (h) are the corresponding best registration results selected by our SAEM automatically, (d) and (i) are local initial registration results while (e) and (j) are global final registration results, respectively. The zoom-in regions on (e) and (j) are shown obviously more precise of aligned vessels than those corresponding regions on (d) and (i) respectively, indicating that the effectiveness and robustness of our two-stage local-to-global registration strategy.

Bifurcation, which obviously indicates that the Cycle-Vessel-Bifurcation feature is the most robust and accurate for registration with the highest SR and the lowest SAEM.

Features	SR	SAEM (pixel)
Cycle	96.73%	0.938
Cycle-Vessel (local)	97.39%	0.903
Cycle-Vessel-Bifurcation (local-to-global)	**100%**	**0.858**

Table 2. Comparison of different features.

At last, we compare our proposed method for retinal image registration with state-of-the-art structure-matching registration methods: Bifurcation structure [6, 5] and Bifurcation structure with global fine registration [19]. This experiment is also applied on the 155 pairs of retinal images under the optimal $M_i N_j L_k$ with minimum $SAEM_{ijk}$. Besides, we also implement our multiscale strategy with SAEM optimal selection on the compared two methods. The results are shown in Table 3, and it can be seen that our method greatly outperforms the other methods in terms of robustness and accuracy with the highest 100% SR and the lowest 0.858 pixel SAEM respectively. Moreover, the proposed mutiscale and SAEM strategy dramatically improves the compared two methods, which also shows the effectiveness and robustness of our intelligent registration based on multiscale selection automatically.

Methods	SR	SAEM (pixel)
Bifurcation structure	50.32%	1.009
Bifurcation structure + Global	59.35%	0.978
Bifurcation + Multiscale + SAEM	95.48%	0.938
Bifurcation Global + Multiscale + SAEM	96.77%	0.877
Our method	**100%**	**0.858**

Table 3. Comparison of different methods.

7. Conclusion and Future Work

In this paper, we address the issues related to the description, matching as well as registration of the vascular structure in retinal images. The contribution of this paper is threefold: 1) a novel stable cycle structure is proposed for retinal vasculature description and an effective and fast Angle-based Depth-First Search algorithm is developed for finding minimum cycle basis; 2) the cycle structure is extended from local to global for robust and accurate matching; 3) the Skeleton Alignment Error Measure is defined to measure and evaluate the registration intelligently. The proposed feature and method can be used for other applications such as retina identification and verification, and also other vascular-related study.

In future work, we will test the method in larger and more natural retinal image datasets, and tune the algorithm for real applications helping the ophthalmologists to analyze and diagnose retina-related diseases.

Acknowledgements

This work was supported by the National Natural Science Foundation of China under Grant Nos. 61271406, 61301240, 31302182.

References

[1] A. Bhuiyan, E. Lamoureux, B. Nath, K. Ramamohanarao, and T. Y. Wong. Retinal image matching using hierarchical vascular features. *Computational Intelligence and Neuroscience*, 2011:9, 2011. 2

[2] A. Can, C. V. Stewart, B. Roysam, and H. L. Tanenbaum. A feature-based, robust, hierarchical algorithm for registering pairs of images of the curved human retina. *IEEE Transactions on Pattern Analysis and Machine Intelligence*, 24:347–364, 2002. 1

[3] A. C. Cassell, J. C. D. Henderson, and K. Ramachandran. Cycle bases of minimal measure for the structural analysis of skeletal structures by the flexibility method. *Proceedings of the Royal Society of London A: Mathematical, Physical and Engineering Sciences*, 350:61–70, 1976. 2

[4] T. Chanwimaluang, G. Fan, and S. R. Fransen. Hybrid retinal image registration. *IEEE Transactions on Information Technology in Biomedicine*, 10:129–142, 2006. 1

[5] L. Chen, X. Huang, and J. Tian. Retinal image registration using topological vascular tree segmentation and bifurcation structures. *Biomedical Signal Processing and Control*, 16:22–31, 2015. 1, 7

[6] L. Chen, Y. Xiang, Y. Chen, and X. Zhang. Retinal image registration using bifurcation structures. In *Proceedings of the 18th IEEE International Conference on Image Processing*, pages 2169–2172, Brussels, September 2011. Institute of Electrical and Electronics Engineers. 1, 7

[7] J. C. de Pina. *Applications of Shortest Path Methods*. PhD thesis, University of Amsterdam, 1995. 2

[8] P. M. Gleiss. *Short cycles: minimum cycle bases of graphs from chemistry and biochemistry*. PhD thesis, University of Vienna, 2001. 2

[9] R. Gould. *Graph Theory*. Dover Publications, 2012. 2

[10] S. M. Lajevardi, A. Arakala, S. A. Davis, and K. J. Horadam. Retina verification system based on biometric graph matching. *IEEE Transactions on Image Processing*, 22:3625–3635, 2013. 2

[11] F. Laliberté, L. Gagnon, and Y. Sheng. Registration and fusion of retinal images–an evaluation study. *IEEE Transactions on Medical Imaging*, 22:661–673, 2003. 1, 6

[12] K. Mehlhorn and D. Michail. Minimum cycle bases: Faster and simpler. *ACM Transactions on Algorithms*, 6:8, 2009. 2, 4

[13] F. P. M. Oliveira and J. M. R. S. Tavares. Medical image registration: a review. *Computer Methods in Biomechanics and Biomedical Engineering*, 17:73–93, 2014. 1

[14] M. Ortega, M. G. Penedo, J. Rouco, N. Barreira, and M. J. Carreira. Personal verification based on extraction and characterisation of retinal feature points. *Journal of Visual Languages & Computing*, 20:80–90, 2009. 6

[15] M. Ortega, M. G. Penedo, J. Rouco, N. Barreira, and M. J. Carreira. Retinal verification using a feature points-based biometric pattern. *EURASIP Journal on Advances in Signal Processing*, 2009:2, 2009. 6

[16] E. Peli, R. A. Augliere, and G. T. Timberlake. Feature-based registration of retinal images. *IEEE Transactions on Medical Imaging*, 6:272–278, 1987. 1

[17] G. P. Penney, J. Weese, J. A. Little, P. Desmedt, D. L. G. Hill, and D. J. Hawkes. A comparison of similarity measures for use in 2-d–3-d medical image registration. *IEEE Transactions on Medical Imaging*, 17:586–595, 1998. 1

[18] A. Perez-Rovira, R. Cabido, E. Trucco, S. J. McKenna, and J. P. Hubschman. RERBEE: robust efficient registration via bifurcations and elongated elements applied to retinal fluorescein angiogram sequences. *IEEE Transactions on Medical Imaging*, 31:140–150, 2012. 1

[19] B. Shen, D. Zhang, and Y. Peng. Blood bifurcation structure and global to local strategy based retinal image registration. In *Proceedings of the 5th Chinese Conference on Pattern Recognition*, pages 394–403, Beijing, China, September 2012. Springer Berlin Heidelberg. 1, 7

[20] C. V. Stewart, C.-L. Tsai, and B. Roysam. The dual-bootstrap iterative closest point algorithm with application to retinal image registration. *IEEE Transactions on Medical Imaging*, 22:1379–1394, 2003. 1, 6

[21] S. Umeyama. Least-squares estimation of transformation parameters between two point patterns. *IEEE Transactions on Pattern Analysis and Machine Intelligence*, 13:376–380, 1991. 5

[22] Y. Wang, G. Ji, P. Lin, and E. Trucco. Retinal vessel segmentation using multiwavelet kernels and multiscale hierarchical decomposition. *Pattern Recognition*, 46:2117–2133, 2013. 2

[23] F. Zana and J.-C. Klein. A multimodal registration algorithm of eye fundus images using vessels detection and hough transform. *IEEE Transactions on Medical Imaging*, 18:419–428, 1999. 1, 5